SAE International

2012-01-0363
Published
04/16/2012

Measurement and Prediction of Filtration Efficiency Evolution of Soot Loaded Diesel Particulate Filters

Danhong Zhong, Suhao He, Pushkar Tandon, Maxime Moreno and Thorsten Boger
Corning Inc

doi:10.4271/2012-01-0363

ABSTRACT

Experimental and theoretical methods are presented to characterize the transient filtration efficiency (FE) behavior of Diesel Particulate Filters (DPFs) exposed to soot laden exhaust gas streams under laboratory and engine exhaust conditions. A (1+1) dimensional transient model, comprising a one dimensional channel model in combination with a one dimensional wall microstructure model is presented to study the sensitivity of the FE behavior on DPF microstructure and geometry properties, along with the impact of the hydrodynamic and aerosol flow conditions (flow rate, temperature, aerosol characteristics). The dynamic model also considers the dynamic soot oxidation by passive regeneration. The model has been validated through use of an extensive set of experimental data obtained under different operating conditions and with DPFs of different microstructure. Evolution of dynamic FE under dynamic engine operating conditions, including the typical emission cycles (FTP, WHTC, etc.) is predicted and the results are compared with the experimental measurements of mass based filtration efficiency. In general, the predictions from the model have been found to be in good agreement with the experiments.

INTRODUCTION

Diesel Particulate Filters (DPFs) are being extensively used in diesel after-treatment systems for removal of particulate matter from the exhaust gas ([1],[2],[3]). Among the various designs proposed for this application, wall-flow filters have proven to be the most effective having high filtration efficiency, low pressure drop and good regeneration characteristics ([4]-[5]). The filtration performance of wall-flow filters depends on a number of factors including the filter microstructure (pore size distribution, porosity) and geometric (DPF diameter and length, cell density, wall thickness) properties, as well as the testing flow and temperature conditions. Furthermore, the DPF filtration efficiency (FE) evolves as the soot is deposited in the DPF, with the deposited soot itself acting as the filtering medium. With continued tightening of the soot exhaust specifications, it is clear that accurate methods to estimate the filtration efficiency characteristics of DPFs are essential. For example, these methods are critical for engineers in identifying the appropriate filter design for the application of interest. Furthermore, these methods should also have the capability to predict the filtration performance under dynamic conditions encountered under vehicle field operation. A number of studies have been undertaken for characterizing filtration efficiency of clean and soot loaded DPFs. Konstandopoulos et al. [6] and Zhang et al. [7] have discussed some elements of the wall microstructure evolution and corresponding filtration efficiency during filtration process. Experimental studies of Liu et al. [8], Ohara et al. [9] and Mizutani et al. [10] have measured FE on DPF systems, but their methods do not have the resolution to capture the complete FE evolution accurately. Recently, Tandon et al. [11] presented a laboratory experimental method and described a transient one-dimensional model for the soot deposition across the thickness of the wall (x-direction) and the corresponding evolution of filtration efficiency with soot loading. The impact of the flow field inside and along the channel (z-direction) had not been considered. Instead the model presented in their paper assumed that the flow can be represented by a constant average flow rate at all axial locations in the filter channel. While this model provides for predictions that are in good agreement with experimental observations for filtration efficiency evolution under well defined steady state laboratory environment, it has limitations for dynamic time varying real exhaust gas conditions and for conditions where significant passive regeneration of the deposited soot layer is occurring. To simulate the filtration

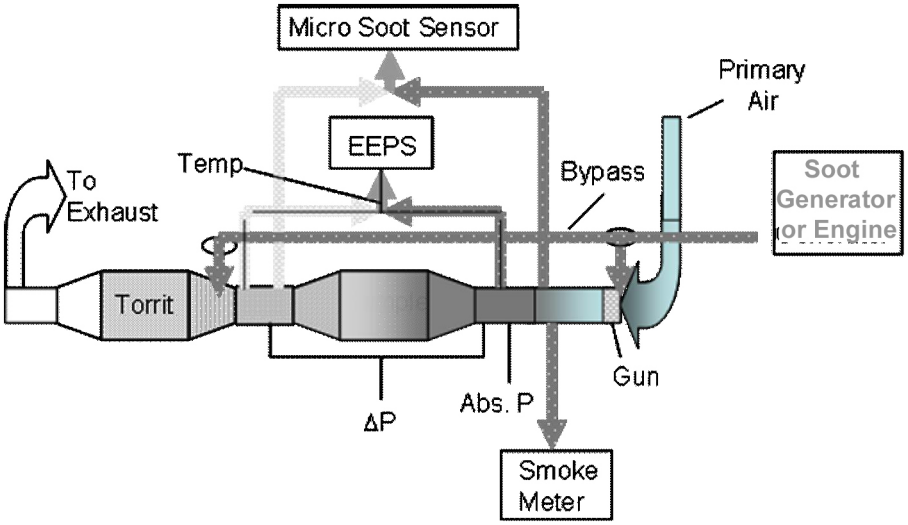

Fig. 1. Schematic of the filtration measurement system [11].

performance under such conditions, in the present paper we describe two extensions of the original model described in [11]. On the one hand we have included the flow and concentration field along the z-direction (axial position along the channel length), we have also included soot oxidation reactions. These additions are essential to be able to simulate the transient filtration behavior of DPFs operating under real exhaust gas conditions.

While the methods we present are successfully able to capture the filter performance under laboratory and field conditions, it is also important to develop simple correlations that can provide design criteria for meeting different engine platforms and exhaust specifications. Hence, in addition to the detailed model, we have also developed a reduced and simplified model leading to a characteristic parameter that enables a simple correlation and assessment of the filtration efficiency of a clean DPF. The latter is particularly useful for practicing engineers to develop design rules for modifying clean filter characteristics for meeting different engine conditions and filtration specifications.

LABORATORY AND ENGINE TESTING OF FITRATION PERFORMANCE OF DIESEL PARTICULATE FILTERS

The setup for a generic filtration efficiency measurement system is shown in Fig. 1. The setup involves testing of the filtration efficiency performance of a DPF either under laboratory setting or on an engine. In the laboratory, the generation of soot is achieved using for example a propane burner (see, e.g., Reproducible Exhaust Simulator (REXS burner) or CAST burner, Matter Engineering Inc.; see, e.g., www.matter-engineering.com/PDF%20Page/REXS-Web.pdf) that is then mixed with the primary air before it is introduced to the input pipe to the DPF. The choice for the soot concentration levels and the primary air flow rates are made such that the total gas mass flow rates are similar to ones encountered in typical light-duty and heavy-duty Diesel engine applications. For engine testing, a similar testing set-up is used, except the soot generator is replaced with an engine. For the testing results presented here, a modern heavy-duty engine designed for US markets is used. Temperature and differential pressure measurements are also performed across the DPF. To estimate the mass based filtration efficiency, soot mass concentrations are measured upstream and downstream of the filter using AVL® 415S Smokemeter (SM) and AVL® 483 photo-acoustic micro-soot sensor (MSS) respectively. The Smokemeter has the capability to measure soot concentration every two minutes, which is sufficient for upstream measurements as the concentration upstream does not change appreciably during the course of the test. The photo-acoustic micro-soot sensor has the capability to measure soot concentration every second and that capability is critical in resolving the dynamic filtration behavior of DPFs. The measurements by the MSS were also seen to be in agreement with DPF "hot weight" measurements and infact demonstrated better resolution and repeatability than the hot weight measurements. In case of experiments in which transient inlet conditions are used, either in the laboratory or on engine, the Smokemeter has been replaced by a second micro-soot sensor.

Laboratory and engine testing of DPFs were performed on experimental DPFs with a broad range of geometric and microstructural properties, and widely varying operating conditions. The filter wall median pore size (MPS) ranged between 9.8 to 28 μm, while the porosity of the wall ranged between 42% and 66%. The DPFs had geometric properties ranging between 4.66-10.5″ diameter, 4.5″-10″ length,

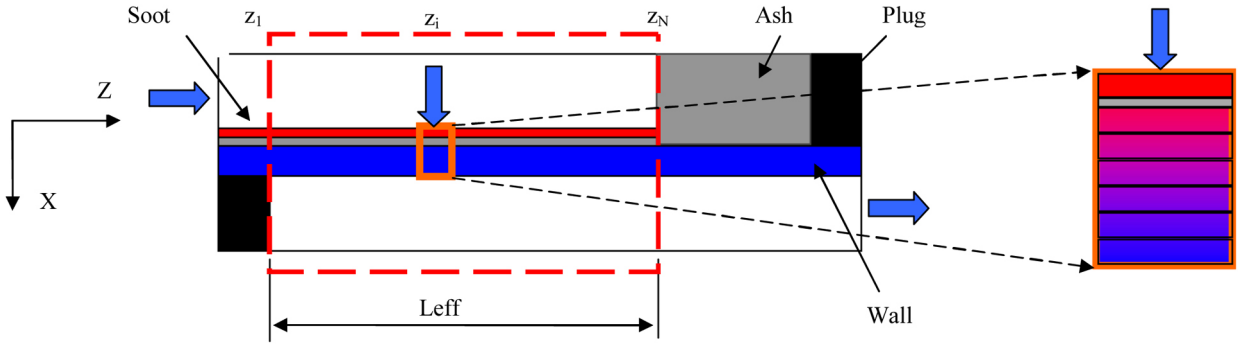

Fig. 2. Schematic of the current 1+1D filtration model, considering channel/wall-flow and soot/ash/wall layers.

203-478 microns wall thickness and CPSI between 180 and 300. The DPFs were tested between standard flow rates of 11 and 680 m^3/hour with the upstream soot concentrations covering almost 2 orders of magnitude. Laboratory experiments have been performed with different mean particle sizes, ranging from ~60 - 120 nm in the upstream feed gas. Measurements of the filtration efficiency for clean and soot loaded DPFs used to validate the mathematical model are presented in the MODEL VALIDATION section below.

DETAILED MATHEMATICAL MODEL

Shown in Fig. 2 is a schematic representation of the unit cell considered to represent the filtration performance of a wall-flow Diesel Particulate Filter. The unit cell is comprised of half of the inlet channel, the filter wall and half of the outlet channel. We define dimension z as the axial direction along the filter length and x as the direction from the inlet to the outlet channel, across the wall (i.e. perpendicular to z). Although the full problem can be described by a 2 dimensional model in z and x we are making the following assumptions, reducing the complexity of the problem without significant loss in physics.

a). For the inlet and outlet channels (gas phase), we are assuming homogeneous concentration and temperature profiles in x direction, reducing the governing equations for each of the two channels to 1 dimensional equations in z direction.

b). Within the wall phase we are considering changes along the filter length (z) as well as across the wall (x). However, we assume that transport occurs primarily from and to the channels (x) and we can neglect mass, energy and momentum transport in z-direction.

The above assumptions result in a model having 1D + 1D character, with one dimension being along the filter axis z and the other being across the wall x. As can be seen from Fig. 2, we not only consider the deposition of soot inside the wall, but also the formation of a soot cake layer onto the inlet channel wall. Accumulation of ash is considered and is important as we use the model to assess the filtration behavior under real world operating conditions with ash being accumulated during the life of the DPF.

In the following sections we describe the governing equations used to describe the interplay between the flow field, the filtration mechanisms and the soot oxidation reactions.

1. FLOW FIELD MODEL

The flow field inside the channel is determined by solving the mass and momentum balance equations. The unsteady terms within the gas phase are assumed to be negligible and the transient soot deposition simulation is based on the updated solution of the steady state equations. The steady state continuity and momentum balance equations in the inlet and outlet channels are given by Eqs. (1), (2), (3), (4) below:

$$\frac{d[u_{in}(dh_{in}-2t_a-2t_s)^2]}{dz} = -4dh_{in}u_w \qquad (1)$$

$$\frac{du_{out}}{dz} = \frac{4dh_{in}}{(dh_{out})^2}u_w \qquad (2)$$

$$\frac{dp_{in}}{dz}(dh_{in}-2t_a-2t_s)^2 = -\frac{d[\rho_{in}u_{in}^2(dh_{in}-2t_a-2t_s)^2]}{dz} - F_{in}\mu u_{in} \qquad (3)$$

$$\frac{dp_{out}}{dz}(dh_{out})^2 = -\frac{d[\rho_{out}u_{out}^2(dh_{out})^2]}{dz} - F_{out}\mu u_{out} \qquad (4)$$

with the wall velocity, u_w, given as:

$$u_w = \frac{p_{in} - p_{out}}{A} \tag{5}$$

where

$$A = \mu\left(\frac{t_w}{k_w} + \frac{dh_{in}}{2k_s SCF_s}\ln\frac{dh_{in} - 2t_a}{dh_{in} - 2t_a - 2t_s} + \frac{dh_{in}}{2k_a}\ln\frac{dh_{in}}{dh_{in} - 2t_a}\right) \tag{6}$$

In Eqs. (1), (2), (3), (4), u is the channel flow velocity, dh is the channel hydraulic diameter, p is the pressure in the channels, and ρ is the gas density in the channel, F is the friction coefficient, with the subscript *in* representing inlet and *out* for outlet channels. Parameters t_a and t_s are the thickness of the ash and soot layers in the channel wall and μ is the gas viscosity. The wall velocity, u_w, is dependent on the differential pressure between the inlet and outlet channels as defined by Darcy's Law (Eqs. (5)-(6)), with t_w as the wall thickness, k_w, k_s and k_a representing the permeabilities of the wall, soot and ash layer, respectively, and SCF is the Stokes Cunningham factor. The permeabilities parameters k_w, k_s and k_a are estimated using the Happel correlation [11] and are a function of local porosity and pore size. In the numerical model the channel length is discretized along the z-direction into M elements to obtain the axial profiles for the variables u_{in}, u_{out}, p_{in}, and p_{out}. To solve Eqs. (1), (2), (3), (4), (5), (6) the following boundary conditions are used:

$$u_{in}(z_1) = \frac{\dot{m}/(\rho_{in} N_c)}{(dh_{in} - 2t_a(z_1) - 2t_s(z_1,t))^2} \tag{7}$$

$$u_{out}(z_1) = 0 \tag{8}$$

$$p_{out}(z_n) = p_{ref} \tag{9}$$

$$u_{in}(z_n) = 0 \tag{10}$$

where $\dot{m}$ is the mass flow rate and N_c is the number of inlet channels.

2. FILTRATION MODEL

The basic model equations used to describe the filtration within the porous wall have been described by Tandon et al. [11]. Compared to this original model several enhancements have been implemented to facilitate the implementation of soot oxidation reactions. These enhancements also improves description of the filtration in the clean state as well as throughout the transient soot accumulation and oxidation. In the present model soot particles entering the filter channel are considered to be captured in the wall by the mechanisms of Brownian diffusion, particle interception and particle inertia. To capture the local soot concentration and the local filtration behavior along the z and x axis, the filter wall is discretized into M elements along the length in z direction, analogous to the channels, and into N elements in x direction across the wall, analogous to what has been described in [11]. The local filtration efficiency of each element, E_{ij} (with i=1, 2, 3, …… N, j=1, 2, 3, ……M) is a function of the local porosity, pore size and flow velocity at any given time.

For each element E_{ij} is calculated based on the local single collector efficiency, η_{ij}, using the relation described by Lee and Gieseke [12]:

$$E_{ij} = 1 - \exp\left(\frac{-3\eta_{ij}(1-\varepsilon_{ij})dx_{ij}}{2\varepsilon_{ij} d_{c,ij}}\right) \tag{11}$$

where ε_{ij}, $d_{c,ij}$ and dx_{ij} are the porosity, collector diameter and the thickness of element ij, respectively. The single collector filtration efficiency, η_{ij}, is estimated by systematically accounting for the contributions from different deposition mechanisms using the correlations described in [11].

The soot deposition inside a wall-flow DPF can be characterized by two distinct modes, namely the deep bed filtration and soot cake filtration. In deep bed filtration, soot deposits inside the porous filter wall, resulting in local changes of the effective wall microstructure and hence the local filter filtration behavior. Initially starting from a clean DPF, the majority of soot particles are captured by means of deep bed filtration inside the porous wall. This situation changes as the pore space becomes filled with soot particles, resulting in no further soot collection inside the filter wall. At that point the transition to the second mode, the soot cake filtration, takes place with the bulk of the soot collection taking place by deposition of soot particles onto the channel walls of the inlet channel as well as onto already deposited soot particles. The result is the formation of a growing soot cake, which acts as the filtration media with the filtration characteristics being determined by the porosity and mean pore size of the soot deposit.

The model presented in [11] assumed that the "deep bed" filtration can be separated into two distinct stages. During the first stage, the addition of soot in the wall results in a reduction of wall porosity, ε, and an increase in collector

diameter, d_c, without any change in the number of collectors. i.e.:

$$\varepsilon = \varepsilon_0 - \frac{6(1-\varepsilon_d)(1-\varepsilon_0)m_{coll}}{\pi \rho_d d_{c,0}^3} \tag{12}$$

$$d_c = \left(d_{c,0}^3 + \left(\frac{6 m_{coll}}{\pi \rho_d} \right) \right)^{1/3} \tag{13}$$

where m_{coll} is the amount of soot added per initial number of collector, ε_d is the deposited soot layer porosity and ρ_d is the deposit density. The deposit density is estimated by matching the predicted initial increase in filtration efficiency with experimental observations and assuming it to be a constant within this stage. In the second stage of deep bed filtration, some of the pores are closed and are not available for filtration anymore. Hence, during this stage, the wall porosity and mean collector diameter are considered to not change with further soot deposition in the filter, but the collection of soot particles results in a reduction in the number of collectors. Methods to estimate the reduction of collectors and the transition from first and second stage of deep bed filtration (based on a prescribed transition permeability) have been discussed in Tandon et al. [11]. Furthermore, the criterion for the transition from deep bed to cake filtration is defined based on the number of collectors decreasing to a critical number of collectors, $N''_{c,crit}$.

The above formulation using discrete stages has resulted in good agreement between predictions and measured filtration efficiency evolution for conditions where there is no significant soot oxidation occurring. However, for conditions with significant contribution of soot oxidation, local soot depletion can occur in both the soot cake deposited on the wall, as well as the soot deposited inside the pore space of the wall. As a result, under transient conditions the conditions describing the effective filtration efficiency can constantly change between the two stages of deep bed filtration as well as soot cake filtration. For such situations, it is important to define criteria for a smooth transition between different stages and regimes. Hence, the model of Tandon et al. [11] has been modified to allow for such smooth transitions. First, the soot density in the pores has been taken to be a continuous function of particle Peclet number, Pe, i.e.:

$$\rho_d = \rho_d(Pe) \tag{14}$$

where the local particle Peclet number, Pe, is defined by Eq. (15).

$$Pe_i = \frac{u_i d_{c,i}}{D_{BD,i}} \qquad u_i = \frac{u_{w,i}}{\varepsilon_i} \qquad D_{BD} = \frac{SCF\, k_B T}{3\pi \mu d_p} \tag{15}$$

Here, $u_{w,i}$ is wall-flow velocity of the i^{th} layer, D_{BD} is the soot particle diffusivity, d_p is the particle size, T is the temperature, k_B is Boltzmann constant and μ is the gas viscosity. SCF is the Stokes-Cunningham factor accounting for the non-continuum effect and is a function of gas mean free path λ [13, 14]

$$SCF = 1 + \frac{2}{d_p}\left(1.23 + 0.41 e^{\left(-0.88 \frac{d_p}{2\lambda}\right)} \right); \; \lambda = \frac{\mu}{\sqrt{\frac{2P\rho}{\pi}}} \tag{16}$$

Eq. (14) considers higher soot packing density in the pore for higher particle Peclet numbers. As the soot deposits in the pores, the particle Peclet number increases because of the change in porosity and collector diameter. As a result the soot density evolves, allowing for smoother transitions between the different stages of filtration.

In the original model formulation described in [11], it was assumed that the deposition of soot onto the filter walls occurs only once the pore space is saturated (number of collectors reached the critical number), leading to the transition to soot cake filtration. However, in detailed CFD simulation using discrete particle tracking models as described in reference [15] we observed that already during the deep bed deposition mode, a small fraction of the soot is deposited onto the channel walls. Based on this observation we consider here that a (small) fraction of the soot is deposited onto the wall even during the initial deep bed phase.

The evolution of the microstructure of the wall due to soot deposition and of the cake layer is determined by estimating the soot mass captured in any element i at axial location j. Considering that the soot stream at a given axial location has soot concentration of C, the total amount of soot entering the wall in time Δt is given by:

$$\Delta m_j \sim D_{hin} \Delta z u_{w,j} C \, \Delta t \tag{17}$$

Then the amount of soot captured in each zone i in time Δt is given by the following expression:

$$\Delta m_{j,i} = \Delta m_j [E_i * (1 - S_i) + (1 - E_i) * S_{i+1}] \prod_{k=1}^{i-1} (1 - E_k) \quad (18)$$

Parameter S in Eq. (18) represents the fraction of soot deposited in the preceding layer from the current layer and is a function of the local permeability given as:

$$S = e^{a(1-\frac{k}{k_0})} \quad (19)$$

where a and k_0 are constants and k is the local permeability. Eq. (18) not only enables a smooth transition between deep bed and soot cake regime but also maintains mass balance when deeper wall layers reach a saturation point.

3. SOOT OXIDATION MODEL

Under engine operating conditions, soot accumulated within the DPF can be oxidized. Under normal operating conditions with temperatures below 450°C, this primarily occurs by soot reacting with NO_2 present in the exhaust gas. This process of soot oxidation is commonly referred to as passive regeneration since no active measures are undertaken to modify the engine operation to facilitate the soot oxidation. Soot oxidation by oxygen present in the exhaust gas generally takes place at appreciable rates at temperatures in excess of 450°C [16, 17]. Typically the engine operation has to be modified to achieve these conditions to oxidize the soot, which leads to the commonly used term of active regeneration. The present model can capture both soot oxidation mechanisms. However, we will limit the discussion to the description of the reactions implemented for passive soot oxidation since they are of special relevance to the use of DPFs in modern and future heavy-duty diesel engines.

The oxidation of soot based on passive regeneration is determined by solving the convective-reaction-diffusion mass balance equation in a multi-layer model in x-direction (soot, ash, wall) for each numerical wall element along z direction. Details of such a model have been described by He et al. [18], and we have used it to simulate the passive regeneration of deposited soot. A number of studies have looked at the kinetics of passive regeneration of soot (Jacquot et al. [19], Messerer, et al. [20], Jeguirim et al. [21], Lee et al. [22]). The current passive regeneration reaction kinetics is based on the cooperative and direct soot/NOx reaction, used by Jeguirim et al.[21]. Thus, the mechanism for the passive soot oxidation is described by the following reactions:

$$C + (1 - \frac{a_h}{2})NO_2 + \frac{1}{2}(1 - \frac{a_h}{2})O_2 \rightarrow a_h CO + (1 - a_h)CO_2 + (1 - \frac{a_h}{2})NO \quad (20)$$

$$C + (2 - a_l)NO_2 \rightarrow a_l CO + (1 - a_l)CO_2 + (2 - a_l)NO \quad (21)$$

where a_h and a_l are the split ratio between CO and CO_2 in reactions (20) and (21) respectively. Kinetic parameters were determined by matching the predictions from the model with a large set of experimental results. When the wall layer contains an oxidation catalyst, NO is oxidized to NO_2, but the conversion is limited by the thermodynamics, i.e:

$$NO + \frac{1}{2}O_2 \leftrightarrow NO_2 \quad (22)$$

For each layer, a generic governing equation for mass balance can be set up in a non-dimensional form, and is given as:

$$\frac{d^2 y}{d\eta^2} - Pe_g \frac{dy}{d\eta} - R(y - y_0) = 0 \quad (23)$$

where, y is the oxidant (O_2 or NO_2) mole fraction; y_0 and R are terms derived from reaction kinetics; η is the non-dimensional length (x-direction); Pe_g is the Peclet number, defined as:

$$Pe_g = \frac{u\delta}{D} \quad (24)$$

In Eq. (24), u is gas velocity across the layer, δ is layer thickness, D is the oxidant diffusivity in the layer. Eq. (23) can be solved analytically to get the NO_2 species concentration profile for each layer as:

$$y = y_0 + C_1 \exp(r_1 \eta) + C_2 \exp(r_2 \eta) \quad (25)$$

where constants C_1, C_2, r_1, and r_2 are determined by applying appropriate boundary conditions. The NO_2 concentration profile then can be used to estimate the rate of passive regeneration of the soot layer as :

$$R_{i,j} = m_{i,j} M_s a_s \left(\frac{p}{p_0}\right)\left[k_{0,h} e^{-\frac{E_h}{RT}} y_{O_2}^{b} \left(\frac{p}{p_0}\right)^{b} + k_{0,l} e^{-\frac{E_l}{RT}}\right] y_{NO_2,i,j} \quad (26)$$

where $R_{i,j}$ is the local rate of reaction at position ($z=z_i$, $x=x_j$), $m_{i,j}$ is the soot amount, M_s is the molecular weight of the soot, a_s is the specific surface area, $k_{0,h}$ and $k_{0,l}$ are the Arrhenius pre-exponential constants for the cooperative and direct reactions, respectively, E_h and E_l are the activation energies for the cooperative and direct reactions, respectively, p and p_0 are the exhaust and reference pressure, y_{O2} and y_{NO2} are the mole fraction of oxygen and NO_2 species and b represents the order of oxygen in the cooperative reaction. The local amount of soot is estimated as :

$$\frac{d(m_{i,j})}{dt} = \Delta m_{i,j} - R_{i,j} \quad (27)$$

SIMPLIFIED CORRELATION FOR CLEAN FILTRATION EFFICIENCY

The 1D+1D model described in the previous section represents an extension of the previous model capturing more detailed physics and reactions. In this section we also start with the model described in reference [11] but will discuss its reduction to a simple characteristic parameter describing the relationship of characteristic filter and operating parameters on the clean filtration efficiency, corresponding to the filtration efficiency for zero soot loading in the DPF. For developing this correlation, we consider that the filtration performance is dominated by the soot capture by Brownian diffusion. The single collector efficiency due to Brownian motion can be described by the following correlation [11].

$$\eta_{BM} = 4\frac{A_s^{1/3}}{Pe^{2/3}}(1-\varepsilon)^{2/3} \quad (28)$$

In Eq. (28) A_s is a complex function of the porosity of the filter wall. Numerical evaluation of the correlation yields that for the range of porosities relevant for diesel particulate filters, A_s can be reduced to a simple power law in porosity, ε, without significant loss in accuracy, i.e.:

$$A_s \approx 3.214\varepsilon^{-2.697} \quad (29)$$

Similar simplifications can be obtained for the Peclet number by obtaining a simplified approximation of the Brownian diffusivity, Eq. (15) as function of temperature and particle size only. It can be shown that in the relevant temperature range of 100-500°C and particle sizes between 50-200 nm, the Brownian Diffusivity is proportional to the temperature and the inverse of the particle size to the power of 1.88, and is given as Eq. (30)

$$D_{BM} \sim \frac{T}{d_p^2} \quad (30)$$

This allows us to express the Peclet number in the following approximate form:

$$Pe \sim \frac{u_w}{T}\frac{(1-\varepsilon)}{\varepsilon^2} d_{50,pore} d_p^2 \quad (31)$$

In Eq. (31), $d_{50,pore}$ is the median pore size of the filter wall and u_w is the wall velocity. Substitution of terms in Eqs. (28), (29), (30), (31) in (11) yields:

$$\ln(1-E) \sim \frac{T^{2/3}}{d_p^{4/3}} A_{Filt} \quad (32)$$

where A_{Filt} is the filtration characteristic parameter given as Eq. (33),:

$$A_{Filt} = \frac{\varepsilon^{0.43} t_w}{d_{50,pore}^{5/3} u_w^{2/3}} \quad (33)$$

with t_w being the wall thickness. This parameter can be further modified to replace the wall-flow velocity by parameters more commonly used for DPF design, such as space velocity, SV, representing the ratio between flow rate and volume of the filter, and filter cell density, CPSI, as in Eq. (34).

$$A_{Filt} \sim \frac{\varepsilon^{0.43} t_w (CPSI)^{1/3}}{d_{50,pore}^{5/3} SV^{2/3}} \quad (34)$$

This parameter allows finding the impact of the different filter characteristics, showing for example the weak dependence on porosity and the strong dependence on pore size as found in [11]. The parameter also allows evaluating different filter materials and designs in a unified manner as will be shown in the following section.

MODEL VALIDATION

We have used the methods presented in the previous section to simulate the evolution of FE behavior of DPFs under a range of transient experimental conditions involving the accumulation of soot. The predictions from the model are validated against experimental measurements performed on laboratory filtration benches (Tandon et al. [11]) and on the engine over transient test cycles.

1. FILTRATION EFFICIENCY OF CLEAN DIESEL PARTICULATE FILTERS

As mentioned earlier, we have performed measurements on experimental DPFs covering a very broad range of filter microstructure and geometric properties, as well as the operating conditions. The comparison of the model predictions and experimental observations for the clean filter FE is shown in Fig. 3. The data show a very good correlation and agreement over these very broad conditions ranges (filter microstructure (porosity, MPS) and geometric (wall thickness, CPSI, diameter, length) properties, along with operating conditions (flow rate, soot concentration, soot size)), covering experimental clean filtration efficiencies from close to 20% to almost 95%. It is observed that the predicted FE are systematically slightly lower than the measurements, likely due to the fact that filtration efficiency measured at very low soot load levels (used for this analysis) typically exhibit some amount of noise and the filtering can lead to such small differences.

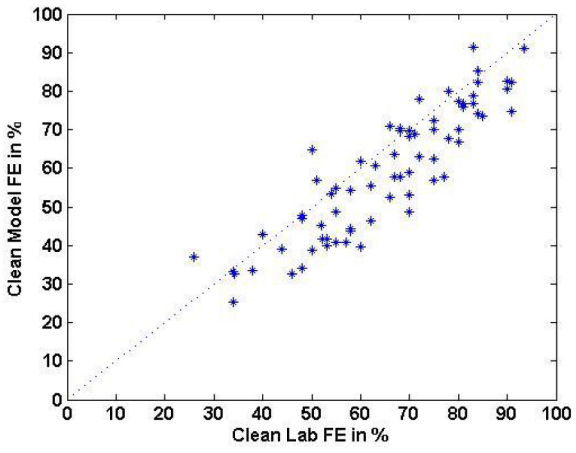

Fig. 3. Model predicted clean FE vs. experimental clean FE obtain in a laboratory filtration bench.

2. CORRELATION BETWEEN SIMPLIFIED FILTRATION PARAMETER AND CLEAN FILTRATION

In Fig. 4, we show the clean filter efficiency of the filters against the simplified filtration characteristic parameter, A_{Filt} derived in the Detailed Mathematical Model section based on Brownian motion collection. The clean filter FE correlates very well with the filter characteristic parameter A_{Filt} (Eq. (34)) over the broad range of filter properties and testing conditions. The excellent correlation between the measured clean filter efficiency and characteristic parameter is surprising considering that the filtration characteristic parameter is based only on the laws of soot capture by Brownian motion and neglects other mechanisms of soot deposition. We propose that this correlation be used as a design tool for optimizing the filter properties for meeting FE requirements for different engine platforms and exhaust specifications. We will also use the information that can be extracted from it in the discussion of the results.

3. EVOLUTION OF SOOT LOADED FILTRATION EFFICIENCY AND VALIDATION WITH LABORATORY MEASUREMENTS UNDER DYNAMIC CONDITIONS

Typical laboratory tests, as described for example in [11], start with a clean filter and then a step change in soot concentration is applied to the DPF. During the experiment the transient response of the filter is monitored. In the experiments described in this section, we have used a modified laboratory test method developed to simulate the flow and soot concentration during a typical light-duty diesel certification test over the New European Drive Cycle (NEDC). The laboratory test also has conditions that represent the four “accelerations” during the urban phase and two during the extra-urban phase. Passive regeneration does not occur during these experiments at room temperature or in the absence of NO_2.

The experiments discussed in this section were done starting with fully regenerated (clean) DPFs. In Fig. 5, we show the laboratory measured FE evolution for two 5.66 in. diameter and 6 in. long filters with different pore structures and geometric properties. The changes in filtration efficiency due to the simulated “accelerations” with the accompanied change in space velocity and soot concentration can be clearly identified. The off-set of these changes with respect to the soot load (“x-axis”) are due to the differences in filtration efficiency, yielding different quantities of trapped soot at the time the “accelerations” occur. Sample A, with a large mean

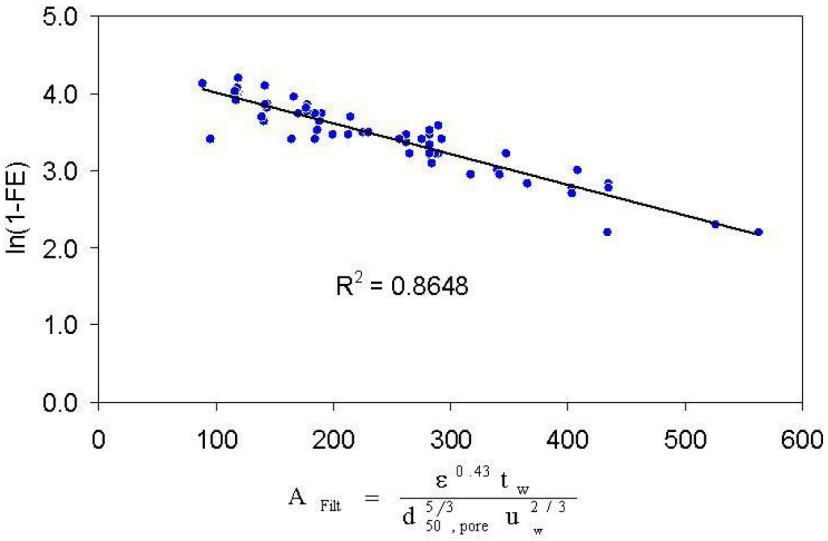

Fig. 4. Experimental clean FE vs characteristic parameter A_{Filt}.

pore size and higher porosity, has the lowest clean filter efficiency and reaches maximum filtration efficiency at relatively high soot loading levels. The low clean filter FE of Sample A is primarily due to the large MPS of the filter wall and it, combined with the larger porosity, results in larger soot load levels at which the FE reaches the maximum efficiency. Sample B has a lower median pore size and porosity compared to Sample A, and also demonstrates higher clean FE than Sample A. It also reaches maximum FE at a lower soot loading of around ~0.15g/L, as explained by its lower porosity. The clean filter efficiency increases and soot load levels corresponding to maximum FE decrease as the MPS and porosity of the filter wall decrease.

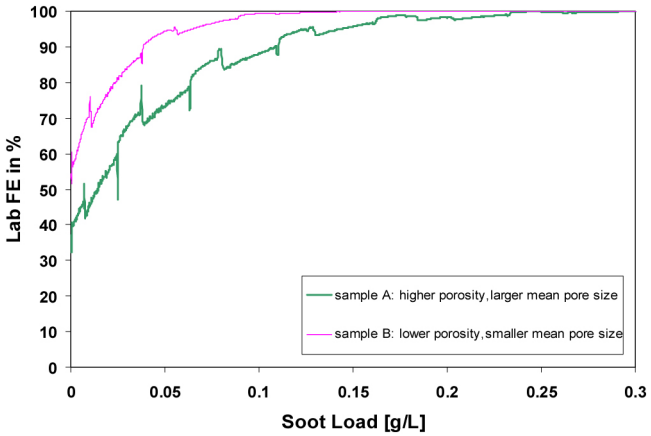

Fig. 5. Measured FE evolution for two different DPFs having different filter microstructure and geometry properties.

Fig. 6 shows the predicted FE evolution with soot loading of these DPFs under the same testing conditions. Comparing the predicted and measured FE behavior, it is clear that despite some differences observed for these examples, the model is successfully able to capture the sensitivity of the FE evolution with filter microstructure/geometry, as well as the transients caused by the variation in the flow rate and the upstream soot concentration.

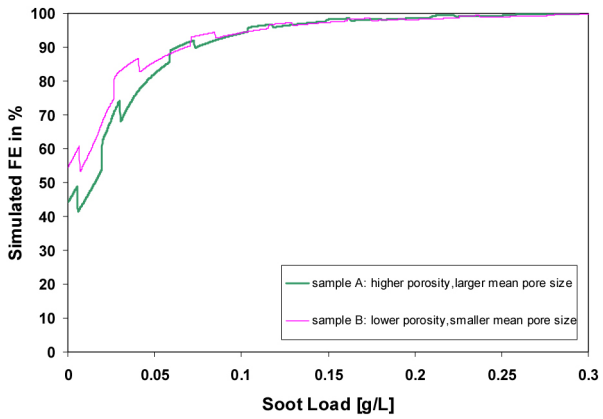

Fig. 6. Model predicted FE evolution for three different DPFs having different filter microstructure and geometry properties.

A direct comparison between FE predictions and measurements for a larger number of samples, covering a wide range of porosities, pore sizes, geometries and test conditions is shown in Fig. 7. Shown are data comparing the absolute difference in the predicted and the measured filtration efficiency when 10%, 30% and 60% of the soot load at which the maximum FE (typically ~100%) is reached for an individual filter (i.e., the absolute value of the soot load at which the maximum FE is reached is different for different filters). The selected values have been found to allow for a good and effective representation of the filtration vs. soot load behavior, facilitating an easier evaluation for a large set

of experiments. The data are plotted vs. the instantaneous particle Peclet number. The instantaneous Peclet number is estimated using Eq. (15), where the soot loaded wall microstructure is based on the first element in z direction and first wall element in wall direction x. The differences observed between the predictions and the experimental measurements are less than 20% over the complete range of Peclet numbers. Some of these differences can also be attributed to deviations in tested filter microstructure and geometric properties from the nominal properties (used in model predictions) of the family of experimental samples.

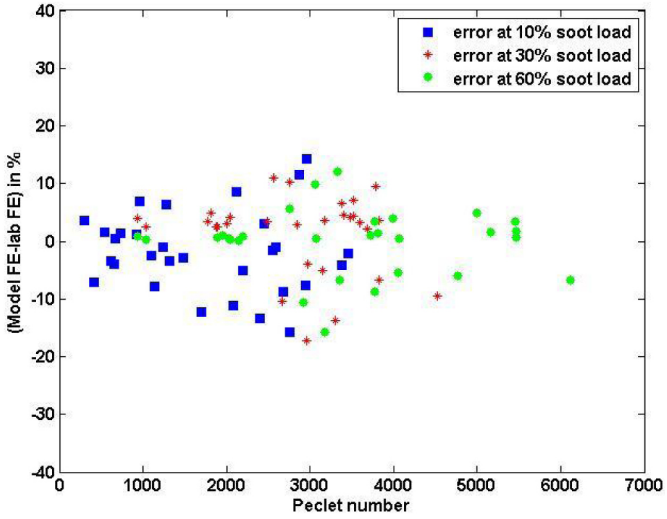

Fig. 7. Difference between model predicted FE and experimental FE at 10%, 30% and 60% of soot load vs the instantaneous particle Peclet number.

RESULTS AND DISCUSSION

In this section we will discuss the application of the new 1D +1D filtration model by means of simulating the filtration behavior of a diesel particulate filter operated on a Heavy-Duty engine over a cold start World Harmonized Transient Cycle (WHTC) followed by two hot cycles with intermediate soak segments. This test cycle represents highly transient conditions with large variations in flow, temperature, gas concentrations and engine out soot emissions. The engine used in the experiments is a modern diesel engine designed for the US market. To obtain information during a test in which soot is accumulated in the filter over the WHTC emission cycles, a calibration was used that enabled conditions with only moderate passive soot oxidation. Testing was done on a transient test bench with data measured at sampling rates of 1 Hz and the DPF was completely regenerated before the start of the test, to allow for a maximum change in filtration efficiency over the cycle. The regeneration was achieved on engine using active regeneration settings at 700 °C for one hour.

In Fig. 8, we show the comparison of predictions and experimental measurements of FE during the transient experiment. As mentioned, the experiments were undertaken on a fully regenerated DPF under cold start conditions and where there was not significant contribution from the passive regeneration. Our methods are successfully able to simulate the transient filtration evolution behavior. The corresponding transient soot concentration downstream of the filter normalized to maximum instantaneous value and the cumulative amount of soot slip normalized to experimental value at the end of the test cycle are shown in Figs. 9 and 10 respectively. While our methods are able to simulate the general dynamic and cumulative behavior well, the predictions are slightly under-predicting the amount of passive regeneration encountered in the experiments, explained by the fact that generic oxidation kinetics have been used and no fine tuning for the DOC and oxidation coating on the DPF has been performed.

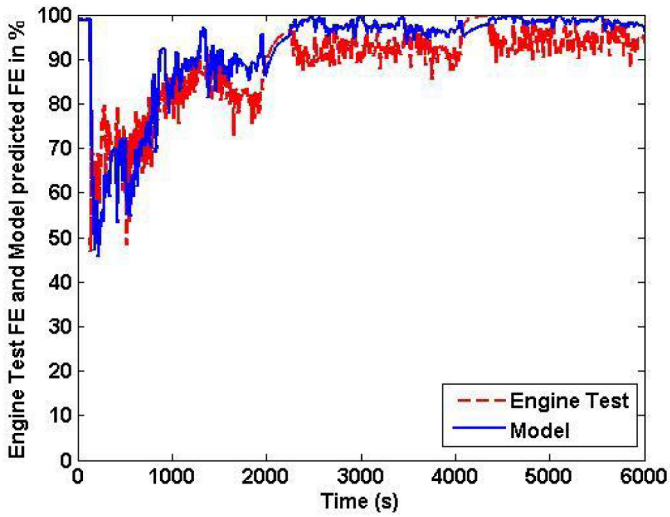

Fig. 8. Predicted and measured FE evolution for WHTC emission cycle

In Fig. 11 is shown the cumulative amount of soot that is entering the DPF (black line) as obtained in the experiment and as used as boundary condition to the filter simulation, along with the predicted values for the soot accumulating inside the wall (green) and onto the wall (pink) as well as the soot slipping through the filter (blue) and the soot oxidized (red). To facilitate the analysis, these quantities have been normalized to the total amount of soot that enters the DPF throughout the cycle.

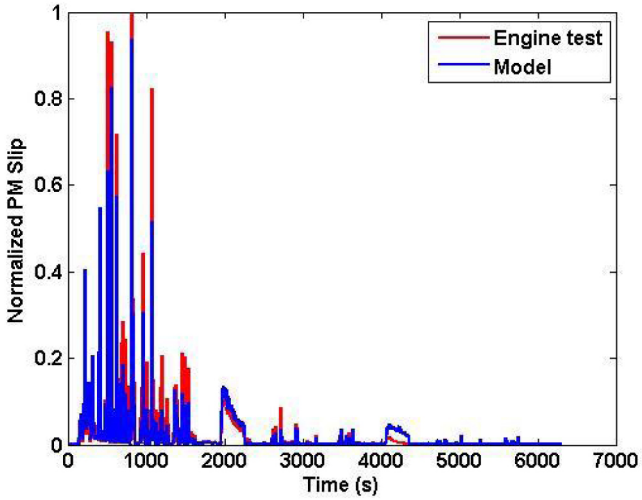

Fig. 9. Predicted and measured PM slip downstream of the filter for WHTC emission cycle

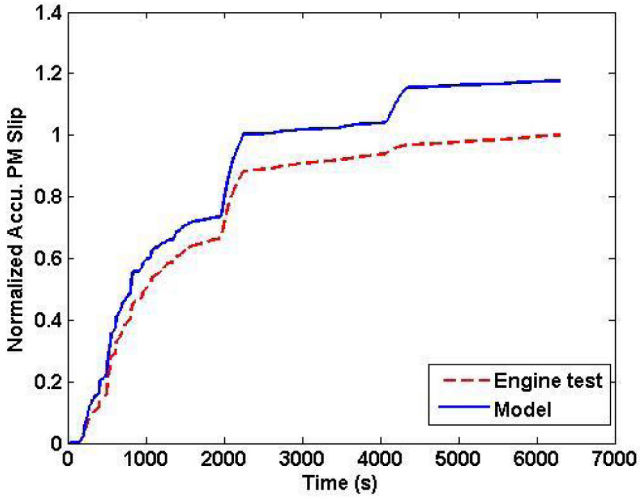

Fig. 10. Predicted and measured soot accumulation in the filter for WHTC emission cycle

A couple of interesting observations can be made from analyzing Fig. 11. The soot deposition, initially occurring primarily inside the wall followed by the deposition onto the wall can be clearly observed from the comparison of the pink and the green line. It is interesting to note that the saturation of the pore space with soot is not completed when the majority of the soot starts to be deposited onto the walls. The effect of passive soot oxidation by NO_2 can be seen to occur only after some time in the cold start cycle (~1700s) when on the one hand the exhaust temperatures become high enough to allow for appreciable conversion of NO to NO_2 over the upstream DOC and on the other hand the local soot concentrations become high enough to result in higher reaction rates, as seen from the change in slope of the line showing evolution of regenerated soot in Fig. 11. At the end of the experiments, after ~6000s, one can observe an enhanced decrease in the soot load inside the wall as well as on the wall. At this stage, there was no additional change in filtration efficiency, since the overall level of soot inside and on the wall remained high.

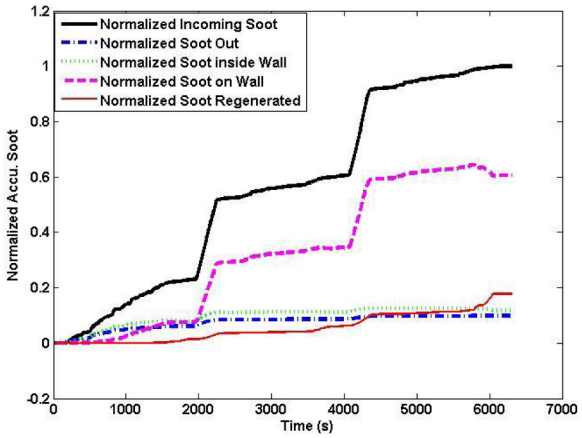

Fig. 11. Total soot accumulation and regeneration for a WHTC cycle.

To demonstrate the effect of axial non-uniformities with a 1D +1D model described in this paper vs. the model described in [11], we show the axial wall-flow velocity, u_w, as function of the axial position in Fig. 12. The data shown are obtained after 180s in the WHTC cycle, when almost no soot is present in the DPF, i.e. the filter is still pretty much in its clean state. The results show the "U-shaped" wall-flow profile commonly observed for clean DPFs, determined by the different pressure losses along the inlet and outlet channel and across the wall. Also plotted as dashed line is the average velocity used in the model described in [11] assuming a uniform axial wall-flow velocity (being equal to 1 for the normalized case). As can be seen from Fig. 12 the rate at which gas flows from the inlet channels to the outlet channels is higher in the inlet and the outlet section and lowest in the middle region of the filter. This results in different local space velocities, which leads to differences in the local (clean) filtration efficiency shown in the right diagram of Fig. 12, as would be expected based on Eq. (32). In the areas of high flow rate, the majority of the initial soot slippage occurs.

The higher local flow rate also impacts the local soot deposition, representing the cumulative local filtration efficiency. This is shown in Figs. 13 and 14. Fig. 13 shows the distribution of the soot collected inside the filter wall (x=0..tw, z=0..L) as predicted by three different models. Model A with 0D in z, assuming a uniform wall-flow velocity along the filter length shows the expected axially uniform soot accumulation. Most of the soot is deposited at the inlet channel side as expected. Model B uses our new 1D +1D approach but the soot oxidation reactions are turned off. One can clearly see the differences in axial soot deposition, as result from the axial flow profile discussed above. A larger

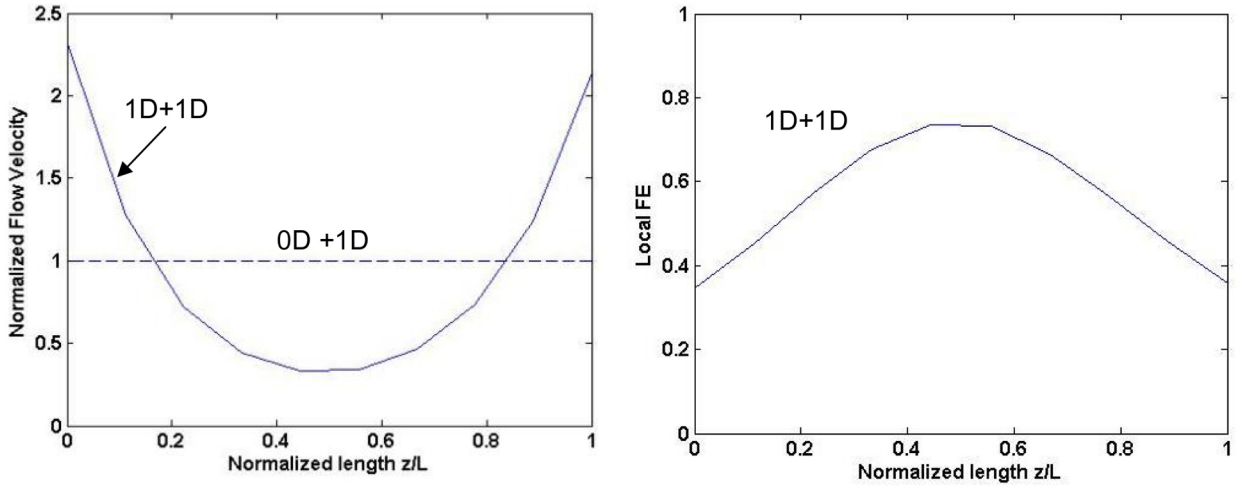

Fig. 12. Normalized axial wall-flow velocity along the filter length (left) and local filtration efficiency along the filter length (right) for the clean filter after 180s. Solid lines are new 1D+1D model. Dashed line represent a model based on uniform wall-flow as described in [11] with updated physics.

fraction of the collected soot is found close to the filter ends, where the highest local wall-flow velocities are observed in the clean state. Model C also uses the new 1D+1D model but the passive regeneration kinetics are active. The comparison between model B and C shows the impact of the passive regeneration, resulting in differences in the local soot loading. Analogous observations can be made from Fig. 14, in which the soot accumulation in the soot cake is shown for the models with 1D(z) + 1D(x) and 0D(z)+1D(x) with and without the soot oxidation kinetics being active. Again, the benefits of the use of the 1D+1D model are obvious as it allows to study the impact of local soot oxidation, resulting in lower local soot deposits. Although not shown here, it is obvious that the effect and the relevance of considering the axial non-uniformity becomes even more important for higher local soot oxidation rates.

SUMMARY/CONCLUSIONS

An experimental and theoretical study has been presented on the filtration efficiency behavior of clean and soot loaded Diesel Particulate Filters (DPFs) operating under transient operating conditions. Filters with a broad range of microstructural and geometric properties have been laboratory and engine tested under very diverse operating conditions. A (1D+1D) dimensional transient model, comprising a one dimensional channel model in combination with a one dimensional wall microstructure model, has been developed and implemented. The model also includes the impact of passive regeneration of the deposited soot layer on the filter soot loading levels and filtration performance. The predictions of filtration efficiency behavior for clean filters, soot loaded filters and performance under transient conditions are in good agreement with the observed filtration efficiency in our laboratory and engine experiments, including in the dynamic cold start WHTC cycle. The benefits of considering axial non-uniformities in flow, soot deposition and, as a result local filtration behavior enable enhanced interpretation of experiments and provide for an excellent tool to study the filtration behavior of different filter concepts under practical conditions. The computational effort required for the 1D+1D model is still low, especially considering the significant enrichment in physics and reaction chemistry. The tool developed thus enables running parametric studies with acceptable computational effort.

A simple filtration correlation parameter has also been developed for clean filter efficiency based on the assumption that Brownian diffusion is the dominant mechanism for soot collection. The correlation between experimentally measured clean filter efficiency has been shown to be in good agreement with the proposed filtration correlation parameter. This correlation is a powerful design tool for practicing engineers to identify the filter characteristics needed for different engines and exhaust specifications.

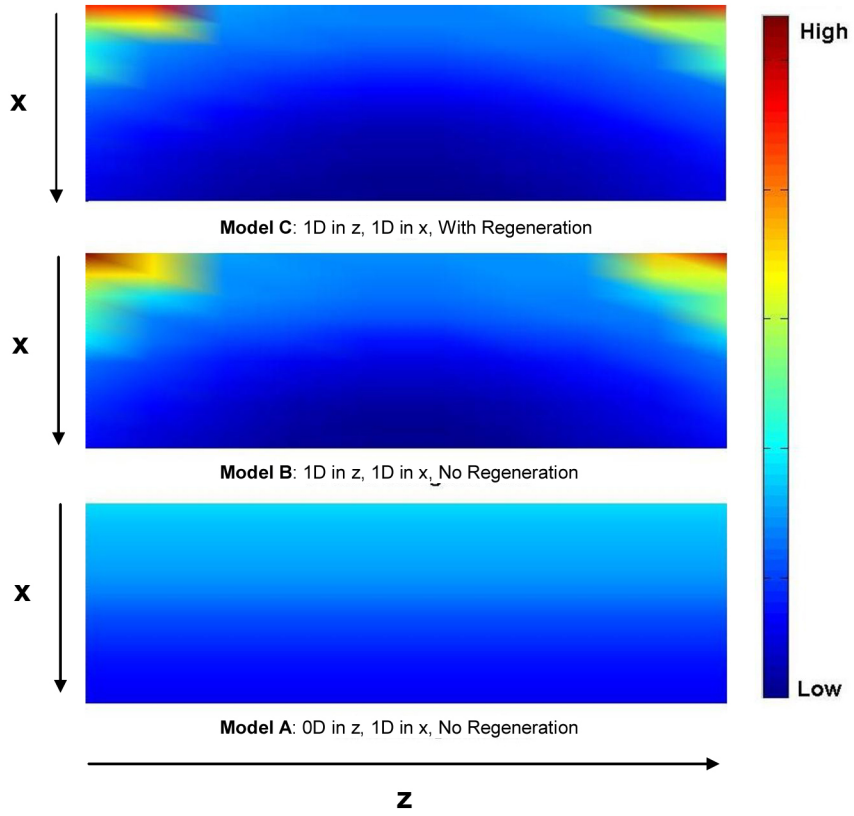

Fig. 13. Soot distribution along the filter and across the filter wall obtained with different models. Note: Inlet channel side is on the top of the individual figures, and wall-flow direction is from top to bottom.

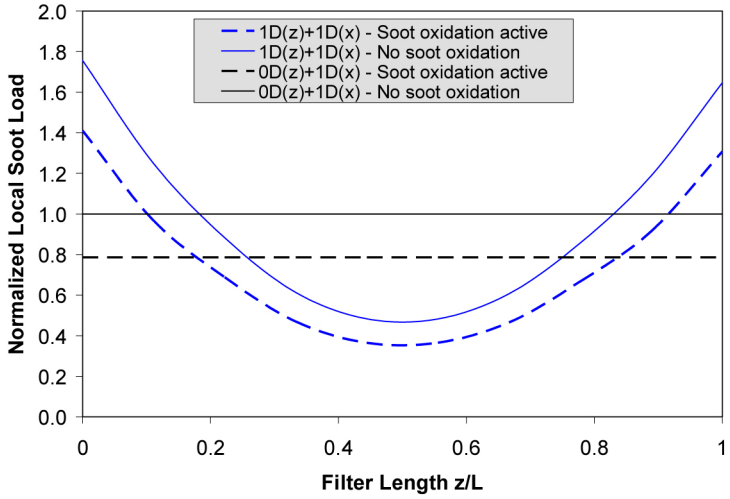

Fig. 14. Soot cake along the filter wall obtained with different models.

REFERENCES

1. Johnson, T., "Diesel Emission Control in Review - The Last 12 Months," SAE Technical Paper 2003-01-0039, 2003, doi:10.4271/2003-01-0039.

2. Johnson, T., "Diesel Emission Control Technology 2003 in Review," SAE Technical Paper 2004-01-0070, 2004, doi: 10.4271/2004-01-0070.

3. Twigg, M. V., "Progress and Future Challenges in Controlling Automotive Exhaust Gas Emissions", *Applied Catalysis B: Environmental* 70 (1-4) 2-15 (2007)

4. Khair, M., "A Review of Diesel Particulate Filter Technologies," SAE Technical Paper 2003-01-2303, 2003, doi:10.4271/2003-01-2303.

5. van Setten, B. A. A. L., Makkee, M. and Moulijn, J. A., "Science and Technology of Catalytic Particulate Filters", *Catalysis Reviews*, 43 (4), 489-564 (2001)

6. Konstandopoulos, A., Kostoglou, M., Skaperdas, E., Papaioannou, E. et al., "Fundamental Studies of Diesel Particulate Filters: Transient Loading, Regeneration and Aging," SAE Technical Paper 2000-01-1016, 2000, doi: 10.4271/2000-01-1016.

7. Zhang, Z., Yang, S., and Johnson, J., "Modeling and Numerical Simulation of Diesel Particulate Trap Performance During Loading and Regeneration," SAE Technical Paper 2002-01-1019, 2002, doi:10.4271/2002-01-1019.

8. Liu, Z., Verdegan, B., Badeau, K., and Sonsalla, T., "Measuring the Fractional Efficiency of Diesel Particulate Filters," SAE Technical Paper 2002-01-1007, 2002, doi: 10.4271/2002-01-1007.

9. Ohara, E., Mizuno, Y., Miyairi, Y., Mizutani, T. et al., "Filtration Behavior of Diesel Particulate Filters (1)," SAE Technical Paper 2007-01-0921, 2007, doi: 10.4271/2007-01-0921.

10. Mizutani, T., Kaneda, A., Ichikawa, S., Miyairi, Y. et al., "Filtration Behavior of Diesel Particulate Filters (2)," SAE Technical Paper 2007-01-0923, 2007, doi: 10.4271/2007-01-0923.

11. Tandon, P., Heibel, A., Whitmore, J. and Kekre, N., "Measurement and Prediction of Filtration Efficiency Evolution of Soot Loaded Diesel Particulate Filters", Chem. Eng. Sci., 65, 4751-4760 (2010)

12. Lee, K. W. and Gieseke, J. A., "Collection of Aerosol Particles by Packed Beds", *Environ. Sci. and Tech.*, 13 (4), 466 (1979)

13. Millikan, R. A., *Phys. Rev.*, Series 2, 22, 1 (1923)

14. Bird, R. B., Stewart, W. E. and Lightfoot, E. N., Transport Phenomena, John Wiley and Sons, New York, (1960)

15. Schermerhorn, A., Khodosevich, K., Joshi, A. and Boger, T., "Detailed Simulation of Exhaust Flow and Deposition of Soot Particles in Porous Particulate Filter Walls", presented at 2nd International Symposium on Modeling of Exhaust-Gas After-Treatment, Bad Herrenalb/Karisruhe (Germany), Sept 19-21, 2011

16. Boger, T., Rose, D., Tilgner, I., and Heibel, A., "Regeneration Strategies for an Enhanced Thermal Management of Oxide Diesel Particulate Filters," *SAE Int. J. Fuels Lubr.* 1(1):162-172, 2009, doi:10.4271/2008-01-0328.

17. Yezerets, A., Currier, N., and Eadler, H., "Experimental Determination of the Kinetics of Diesel Soot Oxidation by O2 - Modeling Consequences," SAE Technical Paper 2003-01-0833, 2003, doi:10.4271/2003-01-0833.

18. He, S., Heibel, A., Shen, M., and George, S., "Mass based methods and systems for estimating soot load", US20110120088A1 (2011)

19. Jacquot, F., Logie, V., Brilhac, J. F., and Gilot, P., Kinetics of the oxidation of carbon black by NO2 influence of the presence of water, Carbon, 40, pp. 335-343, 2002

20. Messerer, A., Niessner, R., Poschl, U., Comprehensive kinetic characterization of the oxidation and gasification of model and real diesel soot by nitrogen oxides and oxygen under engine exhaust conditions: Measurement, Langmuir-Hinshelwood, and Arrhenius parameters, Carbon, 44, pp. 307-324, 2006

21. Jeguirim, M., Tschambar, V., and Ehrburger, P., "Catalytic effect of platinum on the kinetics of carbon oxidation by NO_2 and O_2", *Applied Catalysis B: Environmental*, Vol 76, pp. 235-240, 2007

22. Lee, J., Lee, H., Song, S., and Chun, K., "Experimental Investigation of Soot Oxidation Characteristic with NO2 and O2 using a Flow Reactor Simulating DPF," SAE Technical Paper 2007-01-1270, 2007, doi:10.4271/2007-01-1270.

The Engineering Meetings Board has approved this paper for publication. It has successfully completed SAE's peer review process under the supervision of the session organizer. This process requires a minimum of three (3) reviews by industry experts.

ISSN 0148-7191

SAE Customer Service:
Tel: 877-606-7323 (inside USA and Canada)
Tel: 724-776-4970 (outside USA)
Fax: 724-776-0790
Email: CustomerService@sae.org
SAE Web Address: http://www.sae.org
Printed in USA